Zero loop-area Sagnac interferometer at oblique-incidence for detecting in-plane magneto-optic Kerr effect

X. D. Zhu and Galina Malovichko

Citation: AIP Advances **7**, 055008 (2017); doi: 10.1063/1.4983802
View online: http://dx.doi.org/10.1063/1.4983802
View Table of Contents: http://aip.scitation.org/toc/adv/7/5
Published by the American Institute of Physics

Zero loop-area Sagnac interferometer at oblique-incidence for detecting in-plane magneto-optic Kerr effect

X. D. Zhu[a] and Galina Malovichko
Department of Physics, University of California, Davis, California 95616, USA

(Received 27 January 2017; accepted 8 May 2017; published online 16 May 2017)

We describe a zero loop-area Sagnac interferometer at *oblique incidence* for detecting magneto-optic Kerr effect arising from in-plane magnetization in a sample. By exploiting properties of polarization states under relevant crystal symmetry transformation, we show that contributions from longitudinal and transverse Kerr effects can be separated. In addition we can select one optical arrangement out of four that detects the longitudinal effect with the highest signal-to-noise ratio. Compared to finite loop-area Sagnac interferometers operating at oblique incidence, the zero loop-area interferometer involves significantly fewer optical elements and is thus more stable against drifts in the optical system. For demonstration, we measured the in-plane magneto-optic Kerr effect from a 42-nm Ni film. [http://dx.doi.org/10.1063/1.4983802]

I. INTRODUCTION

Optical detection of magnetic and chiral properties in materials has played an indispensable role in discovery and characterization of novel material phases, mostly for its non-intrusiveness, utility over a wide range of conditions, and compatibility with the concurrent presence of other characterization techniques. Magnetization in a material causes the polarization of an optical beam to change in a way that breaks the time reversal symmetry. Such an effect can be detected in transmission geometry (Faraday Effect) if the sample is sufficiently transparent or in reflection geometry (Kerr Effect) if the sample is opaque or the transmission measurement is not available.[1,2] In practice the linear birefringence is ubiquitous in materials and elements of optical systems and typically produces a much larger effect on the polarization of the optical beam.[1] As a result magneto-optic effects are usually detected by modulating the magnetization and measuring the corresponding polarization change with a suitable method. Such a modulation-based optical detection enables measurements of Kerr rotation as small as 10^{-7} radians.[3] When modulating the magnetization in a sample is not feasible, Kapitulnik, Fejer and coworkers showed that the effect of linear birefringence can be removed efficiently if the magneto-optic effect is measured with a Sagnac interferometer.[4–10] In this case an optical beam and its time-reversed counterpart traverse an identical loop-wise path including reflection from a magnetized sample but in the opposite direction. One then measures the difference of the phases acquired by these two beams. Since the linear birefringence produces a common phase (reciprocal), its effect is essentially absent in the differential phase. Yet the magneto-optic effect yields a non-reciprocal phase in the two beams that has the same amplitude but opposite signs. As a result the differential phase is twice as large as the non-reciprocal phase acquired by one of the two beams.

There are generally two configurations for a Sagnac interferometer: one in which the loop traversed by the two counter-propagating beams encloses a finite area;[4–6] the other in which the loop encloses zero-area (a.k.a. loopless).[7–10] For a finite loop-area Sagnac interferometer, optical beams

[a]Corresponding author, email: xdzhu@physics.ucdavis.edu

are produced through beam-splitting optical elements and configured to being either normally incident or obliquely incident on a sample surface so that effects of magnetization along the surface and perpendicular to the surface can both be measured. Because the two beams are steered separately and eventually recombined before detection, more optical elements are needed, making finite loop-area Sagnac interferometers more subject to imperfection and drift in the optical system in addition to the rotational effect. This has limited the sensitivity for Kerr rotation measurement to 1×10^{-6} radians.[4–6] For a zero loop-area Sagnac interferometer, two optical beams are two orthogonally polarized components of the same original beam and thus require no beam splitting and recombination. As a result, it has shown by Xia *et al.* and Fried *et al.* that such a zero-area Sagnac interferometer can detect Kerr rotation as small as 10^{-7} radians without modulating the magnetization.[7–9] So far though only the normal-incidence geometry has been demonstrated for zero loop-area Sagnac interferometers and in this geometry only the effect from a magnetization perpendicular to the surface can be measured.

We here report a modified zero loop-area Sagnac interferometer in which the optical beams interact with a magnetized sample at oblique incidence such that effects of in-plane magnetization can be detected with same sensitivity. We further show that the extra freedom afforded in this modified interferometer enables us to select polarization states of the beam for optimal detection of longitudinal Kerr effects.

II. OBLIQUE-INCIDENCE ZERO LOOP-AREA SAGNAC INTERFEROMETRY

Figure 1 displays one arrangement of a zero loop-area Sagnac interferometer at oblique incidence. Up to the sample, the arrangement is similar to normal-incidence zero loop-area Sagnac interferometers as reported by Xia *et al.* and more recently by Fried *et al.*[7–9] Briefly, a linearly polarized, collimated broad-band light source centered at 780 nm with a full bandwidth of 30 nm and a power of 6 mW (QPhotonics, Ann Arbor, MI) passes through a 50-50 beam splitter (BS) and a linear polarizer (PL) before being focused into a 1-m polarization-maintaining (PM) fiber. The transmission axis (TA) of PL is aligned to the initial linear polarization of the optical beam and to the slow-axis

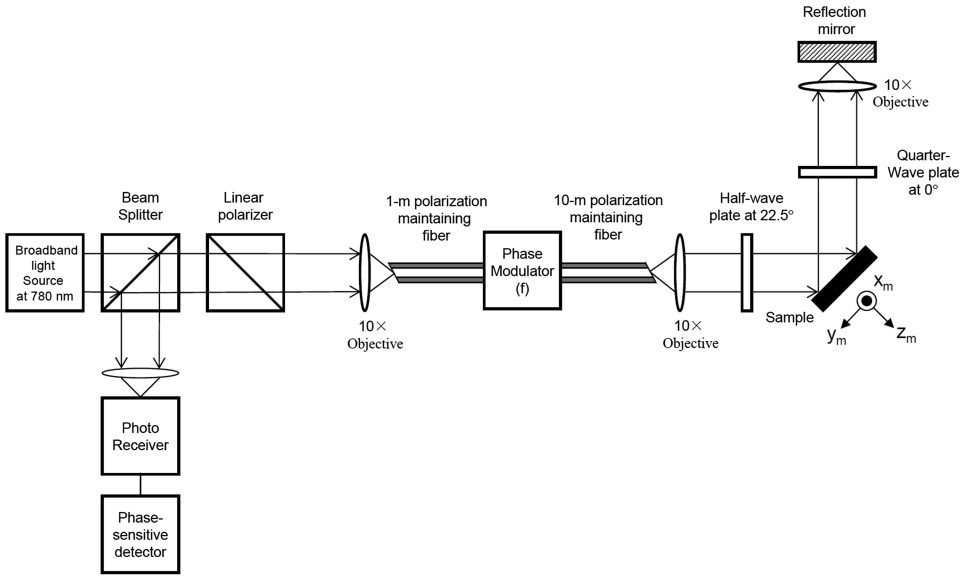

FIG. 1. An arrangement of a zero loop-area Sagnac interferometer for measuring longitudinal and polar Kerr effect of a magnetized sample (a 42-nm Ni film on a silicon wafer in this case). The SA at the input of the 1-m PM fiber is aligned to TA of the linear polarizer. The SA at the output of the 1-m PM fiber bisects TM and TE axes of the electro-optic phase modulator (EOM). The SA at the input of the 10-m PM fiber is aligned to the TM axis of EOM. The SA at the output of the 10-m PM fiber is aligned parallel to the p-polarization with respect to the sample. A portion of the returned beam is directed to a RF photo-receiver and the photocurrent is analyzed with a phase-sensitive detector (SRS844 lock-in amplifier). The axes of magnetization are shown.

(SA) of the 1-m PM fiber. The output of the 1-m fiber is connected to the input of an electro-optic modulator (EOM) such that the SA of the fiber bisects the transverse magnetic (TM) and transverse electric (TE) axes of EOM. EOM is a $LiNbO_3$ phase modulator with V_π = 1.3 volts (EOSPACE Inc, Redmond, WA). V_π is the voltage that induces a phase shift of π to the TM component of the light beam relative to the TE component of the beam. We apply to EOM an f = 4.445 MHz sinusoidal voltage wave form with an amplitude of 0.35V. This causes a phase shift $\Phi(t) = \Phi_0 cos(2\pi ft)$ to the TM component of the beam with Φ_0 = 0.85 radians. The output of EOM is connected to a 10-m PM fiber such that the TM axis of EOM is aligned to the SA of the fiber. The SA of the 10-m PM fiber at the output is aligned to the *p*-polarization with respect to the sample. After the 10-m PM fiber, the beam is collimated with a 10× objective and passes through a half-wave plate (HWP-1) with its SA aligned at 22.5° from the SA of the fiber. The beam is then reflected off the sample at an incidence angle of 50° and passes through a quarter-wave plate (QWP-2) with its SA set parallel to the *p*-polarization after reflection. To complete the loop-wise path, we use a mirror to send the beam back toward the sample again by first focusing the collimated beam with a 10× objective onto the mirror and then having the reflected beam re-collimated by the same objective before sending it back. After going through the same optics but in a reversed order, 50% of the returned beam with an average power of P_{ave} = 4 μW is redirected by the beam splitter (BS) to a 125 MHz photo-receiver (New Focus Model-1801 Newport, CA). The latter has a gain of 4×10^4 V/A and a responsivity of 0.45 A/W at 780 nm. After a calculation based on Jones vectors for the polarization states of the optical beam and Jones matrices for all the optical elements encountered by the beam, the intensity of the beam arriving at the photo-receiver can be shown to vary in time as

$$I(t) = \alpha I_{inc}[\beta + J_1(2\gamma\Phi_0) sin(2\pi ft)\sin(2\theta_K) - J_2(2\gamma\Phi_0) cos(4\pi ft)\cos(2\theta_K) + \cdots] \tag{1}$$

α is essentially an overall throughput of the interferometer including the reflectance of the sample. β is a constant of time near unity. $J_n(2\Phi_0)$ is the n-th Bessel function of the first kind. θ_K is the Kerr rotation angle proportional to the off-diagonal elements r_{ps} and r_{sp} of the reflection matrix as defined by Hunt and by Kapitulnik *et al.*[2,6] $\gamma = sin(\pi f \tau_{round-trip})$ with $\tau_{round-trip}$ being the time it takes the beam to traverse from EOM through the 10-m fiber and the rest of the optical elements that follow including the sample and the reflecting mirror and then back to EOM. The modulation frequency of 4.445 MHz is chosen to make $f\tau_{round-trip} = 0.5$ so that γ is made to unity. The amplitudes of the first harmonic and the second harmonic are then given by $I(f) = \alpha I_{inc} J_1(2\Phi_0)\sin(2\theta_K)$ and $I(2f) = \alpha I_{inc} J_2(2\Phi_0)\cos(2\theta_K)$. They are measured with an SRS844 lock-in amplifier (Stanford Research Systems, Palo Alto, CA). Since θ_K is much smaller than unity, we extract it from the ratio of the first to the second harmonic as

$$\theta_K = \left(\frac{1}{2}\right)\frac{J_2(2\Phi_0)}{J_1(2\Phi_0)}\frac{I(f)}{I(2f)} \tag{2}$$

The choice of $2\Phi_0$ = 1.7 radians maximizes $J_1(2\Phi_0)$ to 0.58 and yields $J_2(2\Phi_0)$ = 0.28. For the arrangement show in Figure 1, the Kerr rotation is caused by the y_m-component (M_y) and the z_m-component (M_z) of the magnetization in the sample as follows,[11]

$$\theta_K = \theta_{K,L} + \theta_{K,P} = Im\left\{\frac{2b(r_{pp} - r_{ss})}{r_{pp}^2 + r_{ss}^2}M_y\right\} + Im\left\{\frac{2c(r_{pp} + r_{ss})}{r_{pp}^2 + r_{ss}^2}M_z\right\}. \tag{3a}$$

Parameter b and c are defined by Kapitulnik *et al.* In this arrangement, α is proportional to $\left|r_{pp}^2 + r_{ss}^2\right|^2$. In the absence of the polar Kerr effect, Equation (3a) is reduced to

$$\theta_{K,L} = Im\left\{\frac{2b(r_{pp} - r_{ss})}{r_{pp}^2 + r_{ss}^2}M_y\right\}. \tag{3b}$$

We can modify the arrangement in Figure 1 to measure the transverse Kerr rotation $\theta_{K,T}$ arising from the x_m-component of the magnetization (M_x) in the surface plane and perpendicular to the plane of incidence. This is done by removing the half-wave plate (HWP-1) before the sample and setting the SA of the quarter-wave plate after the sample to 45° from the *p*-polarization (see Figure S1 in

supplementary material). In this geometry, $\theta_{K,T}$ is related to M_x through[11]

$$\theta_{K,T} = Im\left\{\frac{2a}{r_{pp}}M_x\right\}, \tag{4}$$

with parameter a being defined by Kapitulnik *et al.*[6] In this arrangement α in Equation (1) is proportional to $|r_{pp}r_{ss}|^2$.

In addition to the capability of measuring Kerr effects arising from all three Cartesian components of magnetization in the sample, there is another advantage of the oblique-incidence zero loop-area Sagnac interferometer over normal-incidence Sagnac interferometers. By consideration of polarization states under symmetry operations of C_2 and σ_v,[6,12] we find four combinations of wave plates before and after the sample (including the one shown in Figure 1) that can be used to measure longitudinal Kerr effect. In two of the four combinations, the polarization states are $P_1 = \frac{1}{\sqrt{2}}\begin{bmatrix}1\\1\end{bmatrix}$ and $P_2 = \frac{1}{\sqrt{2}}\begin{bmatrix}1\\-1\end{bmatrix}$; in the remaining two combinations, the polarization states are $P_1 = \frac{1}{\sqrt{2}}\begin{bmatrix}1\\i\end{bmatrix}$ and $P_2 = \frac{1}{\sqrt{2}}\begin{bmatrix}1\\-i\end{bmatrix}$. In these four cases, θ_K's are related to M_y and M_z through different combinations of r_{pp} and r_{ss} and α is proportional to either $\left|r_{pp}^2 + r_{ss}^2\right|^2$ or $\left|r_{pp}^2 - r_{ss}^2\right|^2$.[11] As a result, depending on reflectivities of a sample, namely r_{pp} and r_{ss}, we have the choice to select the one combination out of four that yields the highest signal-to-noise ratio for measuring M_y or M_z. For a 42-nm Ni film, the optimal choice for measuring M_y is the one shown in Figure 1 where $\alpha = \left|r_{pp}^2 + r_{ss}^2\right|^2 >> \left|r_{pp}^2 - r_{ss}^2\right|^2$, and $\left(r_{pp} - r_{ss}\right)\Big/\left(r_{pp}^2 + r_{ss}^2\right)$ is the second largest of four combinations. This option is not available to a normal-incidence zero loop-area Sagnac interferometer. If the sample only has an out-of-plane magnetization along z_m-axis, the optimal choice for measuring M_z (polar Kerr effect) is to remove the quarter wave-plate after the sample and to replace the half-wave plate before the sample with a quarter-wave plate having its SA set to 45° from the *p*-polarization.[11] In this case the polar Kerr rotation is given by

$$\theta_{K,P} = Im\left\{\frac{2c(r_{pp} - r_{ss})}{i(r_{pp}^2 + r_{ss}^2)}M_z\right\} \tag{5}$$

with α in Equation (1) being again proportional to $\left|r_{pp}^2 + r_{ss}^2\right|^2$.

III. EXPERIMENTAL RESULTS AND DISCUSSION

To demonstrate the performance of the zero loop-area oblique-incidence Sagnac interferometer, we measured longitudinal Kerr rotation and transverse Kerr rotation from a 42-nm Ni film deposited

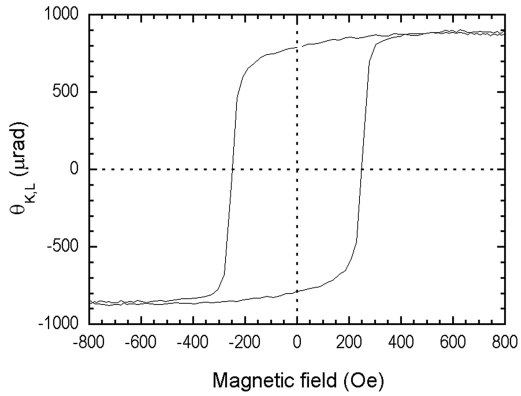

FIG. 2. Longitudinal Kerr rotation angle from a 42-nm Ni film vs. externally applied magnetic field, measured using the zero loop-area Sagnac interferometer at oblique-incidence as shown in Figure 1. The magnetic field is applied along the y-axis in the surface and parallel to plane of incidence. The data are acquired with a lock-in amplifier time constant set to τ = 1 sec.

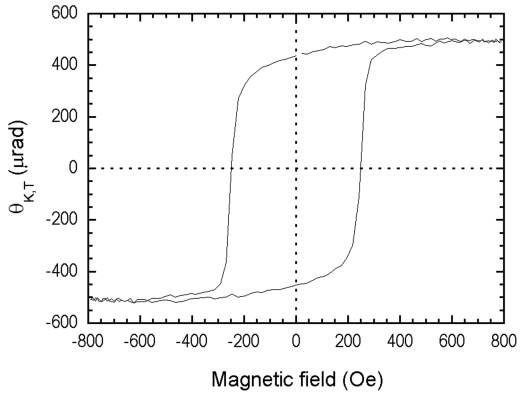

FIG. 3. Transverse Kerr rotation angle from a 42-nm Ni film vs. externally applied magnetic field, measured using a modified zero loop-area Sagnac interferometer at oblique incidence (see the main text and Figure S1 in supplementary material). The magnetic field is applied along the x-axis in the surface plane, namely, the axis that is perpendicular to the plane of incidence.

on a silicon wafer. The Ni film has an easy axis of magnetization in the plane of the film. We use an electromagnet to produce a variable magnetic field up to 1,000 Oe either along the y_m-axis or the x_m-axis in the plane of the film surface. We only expect to observe a longitudinal Kerr effect due to M_y and a transverse Kerr effect due to M_x.

In Figure 2 we show measured $\theta_{K,L}$ from the Ni film when a magnetic field is applied along the y_m-axis of the sample surface (parallel to the plane of incidence). There are 200 data points in each loop. The magnetic field is changed in steps of ~ 20 gausses. The rate of change during step-up and step-down is ~ 20 gauss/sec. After the stepwise change we hold the magnetic field for a few seconds before reading the optical signal with the lock-in amplifier with time constant set to τ = 1 sec. In Figure 3, we show measured $\theta_{K,T}$ from the Ni film when a magnetic field is applied along the x_m-axis of the sample surface (perpendicular to the plane of incidence) with same lock-in amplifier time constant. The data shown are collected in single measurement with no multi-cycle averaging nor oversampling within the single loop data. The high quality of these hysteresis loops demonstrates the notion that a Sagnac interferometer has an inherently low background noise after the birefringence effect in the optical system is suppressed dramatically. Though we do not have a hysteresis loop for the polar Kerr effect from the 42-nm Ni film due to the range of the our present electromagnet (~1000 Oe), one can see from the similarity between Equation (3b) and Equation (5) that the OI ZA-SI can also be used to detect the polar Kerr effect with comparable sensitivity as illustrated in Figure 2.

IV. CONCLUSION

The present zero loop-area Sagnac interferometer at oblique incidence shares the general advantage of zero loop-area Sagnac interferometers by using the two orthogonal polarizing components of an optical beam as "the two counter-propagating beams" instead of using two separate beams. This spares the extra optics and complication associated with the beam splitting and recombination that only add to sources of drifts and noise in a Sagnac interferometer. In fact the optical arrangement as shown in Figure 1 is insensitive to the minute movement of the sample, unlike a finite loop-area Sagnac interferometer at oblique incidence. We measured the noise performance of our present interferometer. We found that the noise has two components: one (±2 μrad/√Hz) is random and comes from the amplifier noise in the photo-receiver (we have only 4 μW at the photo-receiver); the other (±7 μrad) drifts slowly and is due to the residual difference of the reciprocal phases acquired by two "counter-propagating" beams. The photon shot noise is estimated to be ± 0.2 μrad/√Hz for P_{ave} = 4 μW at the receiver, one order of magnitude less than the amplifier noise. The drift can be reduced by more rigidly construction and better beam control after the 10-m PM fiber. The effect of the receiver noise can be lessened by using photo-receivers with significantly lower noise equivalent power (NEP) and/or increasing the power at the receiver (see supplementary material). The minimum detectable

Kerr angle of our present oblique-incidence Sagnac interferometer (~10 μrad/√Hz) is comparable to those of commercially available MOKE ellipsometers (e.g., HO-MOKE **LB**215 from Holmarc) and of the in-situ SMOKE instrument reported by Qiu and Bader.[13]

In summary, we demonstrated a zero loop-area Sagnac interferometer in which the optical beam interacts with a sample at oblique incidence such that Kerr effects from in-plane magnetization in the sample can be measured. The oblique-incidence geometry affords multiple configurations for measuring the longitudinal Kerr effect so that one can choose the one configuration that maximizes the signal-to-noise ratio. Compared to finite loop-area Sagnac interferometers at oblique incidence, the zero loop-area Sagnac interferometer at oblique incidence avoids separating and recombining optical beams and thus has much fewer optical elements. It is thus inherently more stable and promises higher sensitivity to time-reversal breaking effects in a sample, just as normal incidence Sagnac interferometers as reported by Xia *et al.* and Fried *et al.*[7–9]

SUPPLEMENTARY MATERIAL

See supplementary material for an arrangement of OI ZA-SI for detecting the transverse Kerr effect and the characterization of the noises in our present OI ZA-SI.

ACKNOWLEDGMENTS

One of the authors (XDZ) thanks Professor Jing Xia for offering information on fiber-based Sagnac interferometers including his Ph.D. thesis.

[1] Z. Q. Qiu and S. D. Bader, Rev. Sci. Instrum. **71**, 1243 (2000).
[2] R. P. Hunt, J. Appl. Phys. **38**, 1652 (1967).
[3] Y. K. Kato, R. C. Myers, A. C. Gossard, and D. D. Awshalom, Science **306**, 1910 (2004).
[4] S. Spielman, K. Fesler, C. B. Eom, T. H. Geballe, M. M. Fejer, and A. Kapitulnik, Phys. Rev. Lett. **65**, 123 (1990).
[5] S. Spielman, J. S. Dodge, L. W. Lombardo, C. B. Eom, M. M. Fejer, T. H. Geballe, and A. Kapitulnik, Phys. Rev. Lett. **68**, 3472 (1992).
[6] A. Kapitulnik, J. S. Dodge, and M. M. Fejer, J. Appl. Phys. **75**, 6872 (1994).
[7] E. R. Schemm, W. J. Gannon, C. M. Wishne, W. P. Halperin, and A. Kapitulnik, Science **345**, 190 (2014).
[8] J. Xia, P. Beyersdorf, M. M. Fejer, and A. Kapitulnik, Appl. Phys. Lett. **89**, 062508 (2006).
[9] A. Fried, M. Fejer, and A. Kapitulnik, Rev. Sci. Instrum. **85**, 103707 (2014).
[10] J. Xia, Ph.D. thesis, Stanford University, 2008.
[11] X. D. Zhu, unpublished.
[12] A. L. Shelankov and G. E. Pikus, Phys. Rev. B **46**, 3326 (1992).
[13] Z. Q. Qiu and S. D. Bader, J. Magn. Magn. Mater. **200**, 664 (1999).